Journal of Inorganic Biochemistry 203 (2020) 110910

Contents lists available at ScienceDirect

Journal of Inorganic Biochemistry

journal homepage: www.elsevier.com/locate/jinorgbio

An Erlotinib gold(I) conjugate for combating triple-negative breast cancer☆

Enrique Ortega[a], Ana Zamora[b], Uttara Basu[c], Petra Lippmann[c], Venancio Rodríguez[a], Christoph Janiak[d], Ingo Ott[c], José Ruiz[a,*]

[a] Departamento de Química Inorgánica, Universidad de Murcia and Institute for Bio-Health Research of Murcia (IMIB-Arrixaca), E-30071 Murcia, Spain
[b] Department of Chemistry, KU Leuven, Celestijnenlaan 200D, 3001 Heverlee, Belgium
[c] Institute of Medicinal and Pharmaceutical Chemistry, Technische Universität Braunschweig, Beethovenstrasse 55, 38106 Braunschweig, Germany
[d] Institut für Anorganische Chemie und Strukturchemie, Heinrich-Heine-Universität Düsseldorf, Universitätsstr 1, 40225 Düsseldorf, Germany

ARTICLE INFO

Keywords:
Gold(I) conjugate complex
Erlotinib
DNA damage
Reactive oxygen species
Breast cancer
Apotosis

ABSTRACT

An Erlotinib triphenylphosphane gold(I) conjugate has been prepared from $AuCl(PPh_3)$ and its crystal structure has been established by X-ray diffraction, showing a metallo-helicate formation. IC_{50} values of the new gold conjugate were calculated towards a panel of human tumor cell lines representative of breast (MCF-7, MDA-MB-231) and colon (HT-29) cancer cells. Overall, the gold conjugate exhibited higher cytotoxic activity than that of Erlotinib against the cancer cells studied. Particularly, the antiproliferative effect of the conjugate demonstrated to be 68-fold higher than Erlotinib in highly metastatic and triple negative MDA-MB-231 cell line. The gold conjugate caused DNA damage, reactive oxygen species (ROS) increase and induced apoptosis. Flow cytometry analysis showed that the conjugate induces significant arrest in S and G_2/M phases primarily, whereas Erlotinib, as an inhibitor of epidermal growth factor receptor (EGFR), blocks G_1/S transition and increases G_1 cell population.

1. Introduction

Breast cancer is the most frequently diagnosed in females and represents a dominant cause of death in both sexes combined, accounting for 11.6% of the total cancer cases (data corresponding to GLOBOCAN, International Agency for Research on Cancer) [1]. In particular, triple negative breast cancer (TNBC) represents a highly aggressive and metastatic type of cancer whose treatment remains challenging as targeted receptor therapy fails to benefit [2].

Regarding to chemotherapeutic targets, the overexpression of epidermal growth factor and its receptor (EGFR) are considered key hallmarks in certain tumors. Activation of EGFR signaling in tumor cells has been linked with increased proliferation and decreased apoptosis, angiogenesis and metastasis. Therefore, EGFR constitutes an attractive target for the development of anticancer pharmaceuticals [3]. EGFR-targeting compounds such as the FDA-approved Erlotinib entered clinical trials for cancer therapy with success [4]. The mechanism of action of Erlotinib involves the inhibition of EGFR tyrosine kinase activity through an ATP-competitive binding to the kinase domain [4]. The small size and the inhibitory capacity of Erlotinib make it ideal as an organic pharmacophore.

On the other hand, cisplatin and other platinum-based drug therapies are often associated with undesirable side effects such as nephrotoxicity, hearing loss and hemorrhages [5]. Therefore, there is a demanding need for new chemotherapeutic candidates that target TNBC cells in an efficient manner. The concept that EGFR oncogene inhibitor drugs could be used as targeted treatment against TNBC has been put forth based on estimates that 30–60% of TNBC express high levels of EGFR. However, results from phase III clinical trials testing EGFR inhibitors, alone or in combination with platinum chemotherapy, did not improve patient survival [6].

Among the non-platinum drugs, gold compounds have gained increased attention due to the variety of ligands that can be linked to the metal center in its different oxidation states [7]. Stability of the ligands coordinated to metal center is a critical issue for the design of gold-based drugs. Thus, ligands with relatively high bond dissociation energies such as phosphanes, carbenes or alkynes are privileged moieties [8,9]. Moreover, gold(I) complexes of the type $[RC{\equiv}C–Au–PR'_3]$ have shown high antiproliferative activity in tumor cells [10–12], influenced key parameters of tumor cell metabolism [13–17] and triggered anti-angiogenic effects at non-toxic concentrations in zebrafish embryos [18,19]. Whereas the biological mode of action of gold-containing

☆ Dedicated in Memoriam to Professor Dr. Juan Manuel Salas.

* Corresponding author.
E-mail address: jruiz@um.es (J. Ruiz).

https://doi.org/10.1016/j.jinorgbio.2019.110910
Received 6 July 2019; Received in revised form 16 October 2019; Accepted 27 October 2019
Available online 30 October 2019
0162-0134/

drugs is unclear and can display a high variety of targets, it is generally accepted that the strong and selective inhibition of the enzyme thioredoxin reductase (TrxR) is of high relevance for the pharmacology of these metallodrugs.

In this paper, we have used a phosphane gold(I) scaffold to re-orientate the well-established EGFR tyrosine kinase inhibitor, Erlotinib. We hypothesized that complexation of Erlotinib to the metal center could result in either an Erlotinib-conjugate with affinity for its well-known biological target, EGFR, or in a reactive gold complex that enhances the transport of the organic pharmacophore Erlotinib. In fact, Erlotinib-targeted zinc(II) phthalocyanine led to selective photodynamic activity towards EGFR + HepG2 cancer cells [20]. At the time, the resulting conjugate could exert a different mechanism of action towards cancer cells that could improve the activity of Erlotinib towards TNBC cells. The new gold(I)-Erlotinib conjugate was characterized by ^{1}H, ^{13}C NMR, and ESI-MS and X-ray diffraction. The cytotoxicity towards cell lines representative of breast and colon cancer was studied and in order to explore the resulting mechanism of action, flow cytometry analysis and cell-based fluorescent assays were undertaken. Cellular morphology changes were also studied by contrast phase inverted microscopy. In addition, the amount of gold both in whole cells and in DNA was determined by AAS and ICP-MS, respectively.

2. Experimental section

2.1. Instrumental measurements

The C, H and N analyses were performed with a Carlo Erba model EA 1108 microanalyzer. Melting point was determined with a Reichert apparatus. The ^{1}H, ^{13}C, and ^{31}P NMR spectra were recorded on a Bruker AV 600 MHz spectrometer using $SiMe_4$, and H_3PO_4 as standards. ESI mass (+ mode) analyses were performed on a HPLC/MS TOF 6220. Absorption spectra were measured on a Perkin Elmer Lambda 750 S spectrometer. Fluorescence measurements were carried out with a modular spectrofluorometer Fluorolog3–22 Horiba Jobin Yvon with a 450 W xenon lamp.

2.2. Materials

The starting gold complexes [AuCl(tht)] (tht = tetrahydrothiophene) and [AuCl(PPh_3)] were prepared by procedures previously described [21,22]. Solvents were dried by the usual methods. $NaAuCl_4$, KOH, were obtained from Sigma-Aldrich (Madrid, Spain); *N*-(3-ethynylphenyl)-6,7-bis(2-methoxyethoxy)quinazolin-4-amine (Erlotinib) from Beta Pharma Scientific, Inc. (USA).

2.3. Synthesis of [(3-((6,7-bis(2-methoxyethoxy)quinazolin-4-yl)amino) phenyl)ethynyl](triphenylphosphane)gold(I)

To a suspension of Erlotinib (78.89 mg, 0.2 mmol) in MeOH (10 mL) was added KOH (112.22 mg, 2.0 mmol) and stirred for 5 min to obtain a solution. Then, [Au(PPh_3)Cl] (100 mg, 0.2 mmol) was added and the reaction mixture was stirred at RT for 24 h. The white precipitate was filtered and washed with MeOH (2 mL). The solid was treated with CH_2Cl_2 (20 mL) and filtered through a short pad of Celite. The solvent of the filtrate was evaporated to 2 mL and treated with diethyl ether to give a white solid, which was collected by filtration and air-dried. Yield: 56%. Anal. calcd. for $C_{40}H_{37}AuN_3O_4P$: C 56.41, H 4.38, N 4.93. Found: C 56.29, H 4.43, N, 4.84%. Mp: 210 °C. ^{1}H NMR (600 MHz, DMSO-d_6) δ (ppm): 9.38 (s, 1H, NH), 8.47 (s, 1H), 7.88 (s, 1H), 7.86 (s, 1H), 7.65–7.53 (m, 16H), 7.29 (t, J = 7.8 Hz, 1H), 7.21 (s, 1H), 7.05 (d, J = 7.2 Hz, 1H), 4.28 (m, 4H), 3.75 (m, 4H), 3.36 (s, 3H), 3.34 (s, 3H). ^{31}P NMR (242.94 MHz, DMSO-d_6) δ (ppm): 42.12. ^{13}C{1H} NMR (150.92 MHz, DMSO-d_6) δ (ppm): 156.17, 153.70, 152.86, 148.04, 146.93, 139,44, 133.89 (d, J_{CP} = 13.2 Hz, C_{ortho} of PPh_3), 131.94, 129.61 (d, J_{CP} = 11.0 Hz, C_{meta} of PPh_3), 129.25 (d, J_{CP} = 55.7 Hz, C_{ipso} of PPh_3), 128.45, 126.23, 125.21, 124.78, 120.54, 108.90, 108.20, 103.23, 70.11, 70.03, 68.35, 68.01, 58.37, 58.32. ESI^{+} mass spectra (DMF) *m/z* observed: 852.227, 100%; calculated for $[M + H]^{+}$: 852.226.

2.4. X-ray crystal structure analysis

Crystals suitable for X-ray diffraction of the title compound were obtained from dichloromethane/toluene/hexane and mounted in inert oil on a glass fiber and transferred to the diffractometer. Details of the X-ray structure determination and refinement parameters for the compound are given in Tables S1–S3 in the Supporting Information. Intensities were registered at low temperature on a Bruker D8QUEST diffractometer using monochromated Mo $K\alpha$ radiation (λ = 0.71073 Å) in ω scan mode. The structure was solved by direct methods [23]; refinement was done by full-matrix least squares on F^2 using the SHELXL program suite [23]; empirical (multi-scan) absorption correction with SADABS (Bruker) [24]. The site occupation factors of the embedded CH_2Cl_2 solvent molecule were allowed to refine freely and refined to 0.826, to yield the crystallographic formula $C_{40}H_{37}AuN_3O_4P{\cdot}0.413CH_2Cl_2$ Graphics were drawn with DIAMOND [*DIAMOND 4* for Windows; Crystal Impact Gbr, Bonn, Germany, 2016, http://www.crystalimpact.com/diamond].

2.5. Stability assays

The stability of the new conjugate **1** was evaluated by UV/Vis spectrophotometry and NMR spectroscopy. For the UV/Vis studies the conjugate was dissolved in DMF, water/DMF (1:1), or cell culture medium Roswell Park Memorial Institute medium (RPMI)/DMF (1:1) (50 μM) and was measured over 24 h at room temperature. We also verified that the ^{1}H NMR spectrum of a solution of **1** in DMSO-d_6 at room temperature did not change even after 48 h.

2.6. Cell lines and culture

Human breast cancer cells, MCF-7, and the non-tumorigenic kidney cells, BGM, were grown in Dulbecco's Modified Eagle Medium (DMEM) containing 1 g/L glucose supplemented with 10% final concentration of fetal bovine serum (FBS), 2 mM L-glutamine and 0.1 mM non-essential amino acids.

HT-29 colon carcinoma cells, MDA-MB-231 breast cancer cells, MCF-7 breast carcinoma cells were maintained in DMEM (4.5 g/L D-glucose, L-glutamine, pyruvate), which was supplemented with gentamycin (50 mg/L) and fetal bovine serum superior, standardized (Biochrom GmbH, Berlin) (10% v/v), and were passaged once a week. BGM primate kidney cells were maintained in Dulbecco's Modified Eagle Medium (1 g/L D-glucose, L-glutamine) and supplemented with fetal bovine serum (10% v/v). RC-124 human kidney cells were maintained in McCoy's 5A (modified, with L-glutamine) medium which was supplemented with gentamycin (50 mg/L) and fetal bovine serum superior, standardized (Biochrom GmbH, Berlin) (10% v/v), and were also passaged once a week. For experiments with RC-124 cells, microtiter plates had been pretreated in the following way: 30 μL of a sterilized gelatine solution (1.5% (m/v)) were added to each well of flat bottom 96-well plates, the plates were covered with their lids, incubated for 1 h at 37 °C, the excess solution was removed, the wells were washed with PBS 7.4 pH, and the new cell culture medium was added.

All cell lines were cultured in a humidified incubator at 310 K in a 5% CO_2 atmosphere and subcultured 2–3 times a week with an appropriate density for each cell line. The cells lines were confirmed to be mycoplasma-free using Hoechst DNA staining method [25]. The maximum % of DMSO used in cell experiments was 0.4 (except for cisplatin, water diluted).

2.7. Cytotoxicity assays

The antiproliferative effects were determined according to a recently used method with minor modifications [26]. In short: a volume of 100 mL of HT-29 cells (2565 cells per mL), MDA-MB-231 cells (4120 cells per mL), MCF-7 cells (4840 cells per mL) or RC-124 cells (1460 cells per mL) was transferred into the wells of 96-well plates (note: for RC-124 pretreated plates were used, see above) and incubated at 37 °C/5% CO_2 for 72 h (MCF-7, MDA-MB-231, RC-124, BGM) or 48 h (HT-29). Stock solutions of the compounds in DMF were freshly prepared and diluted with the cell culture medium to graded concentrations (final concentration of DMF: 0.1% *v*/v). After 72 h (HT-29) or 96 h (MCF-7, MDA-MB-231, RC-124, BGM) of exposure, the cell biomass was determined by crystal violet staining and the IC_{50} value was determined as the concentration that caused 50% inhibition of cell proliferation compared to an untreated control. Results were calculated as the mean values of three independent experiments.

2.8. Cellular uptake in MDA-MB-231 cells

The cellular metal uptake was determined according to previously described methods [26]. In short: MDA-MB-231 breast carcinoma cells were grown until at least 75–80% confluency in 150 cm^2 cell-culture flasks. Stock solutions of the compounds in DMF were prepared and diluted with cell-culture medium to a final concentration of 2.0 μM immediately before use (final DMF concentration: 0.1% *v*/v). The cell culture medium of the flasks was replaced with the medium that contained the metal compound (20 mL) and the flasks were incubated at 37 °C/5% CO_2 up to 48 h. After the desired incubation period the uptake was stopped by removing the cell culture medium. The cells were washed with PBS (10 mL), the washing solution was removed, and the cells were isolated after 6 min trypsinization (2.4 mL trypsin solution 0.05%, containing EDTA 0.004%) by centrifugation (5 min, 1096 *g*). The obtained cell pellets were stored at −20 °C for further use. For metal and protein quantification the pellets were resuspended in demineralized water (1.0 mL) and lysed for 30 min by ultra-sonication. The protein content of lysates was determined by the Bradford method and the metal content was determined by High Resolution Continuum Source Atomic Absorption Spectrometry (HRCS-AAS) using matrix matched calibration as previously described in more detail [26].

2.9. Cell death assays in tumoral vs normal cells

To check the effect of conjugate **1** on both tumoral and normal cells, MDA-MB-231 and BGM cells were cultured in 6 well plates with $2{\cdot}10^5$ cells/well seeding density. After cell surface attachment, either Erlotinib or conjugate **1** was added at different concentrations (5 or 20 μM). Then, cells were harvested, washed with PBS and stained with a 40 ng/mL propidium iodide solution for 30 mins. Cell events were analyzed by flow cytometry (Becton Dickinson FACSCalibur) acquiring 10,000 events per sample. Data were analyzed using Flowing Software version 2.5.1 using Side Scattered Height (SSH) and FL2-A channels.

2.10. Flow cytometric cell cycle analysis

MDA-MB-231 cells were seeded into 6-well plates at a density of $3{\cdot}10^5$ cells/well. Cells were treated with either 5 or 20 μM of **1**, Erlotinib or cisplatin for 24 h. Then cells were trypsinized, fixed in ice-cold 75% EtOH for 1 h, treated with RNase 1 μg/mL, stained with 40 μg/mL PI for 30 min and analyzed using Becton Dickinson FACSCalibur (λ_{exc} = 488 nm and λ_{em} = 630 nm). Two independent experiments were performed with $n = 2$ yielding similar results.

2.11. DNA-bound gold in cells

MDA-MB-231 cells were in 25 cm^2 cell-culture flask for 96 h until confluency was achieved. Cells were treated with either conjugate **1** or cisplatin (10 μM) for 24 h and lysed in DNAzol reagent (DNAzol®, MRC) supplemented with RNAse A (100 mg/mL). The DNA was precipitated using pure EtOH, washed with 75% EtOH and solubilized in 8 mM NaOH. The DNA content was quantified by UV spectrophotometry measuring A260 (NanoDrop ND 1000 spectrophotometer) and the amount of metal (^{197}Au or ^{195}Pt) was determined by ICP-MS. Two independent experiences were performed ($n = 2$).

2.12. DNA intercalation studies

Competitive DNA intercalation studies were carried out using ethidium bromide (EtBr) displacement assay. Fluorescence of EtBr was monitored (λ_{ex} = 495 nm, λ_{em} = 590 ± 10 nm) at a fixed concentration of calf-thymus DNA (5 μM in Tris-HCl 10 mM pH 7.4) pretreated with 1.5 μM EtBr during titration with increasing concentration of conjugate **1** (0–100 μM) after 2 h incubation. Normalized results of the fluorescence measurements were calculated using percentage of untreated EtBr:DNA samples as 100% (no EtBr fluorescence displacement). Two independent experiments were performed using triplicate points per concentration level.

2.13. Mitochondrial membrane potential perturbation

Mitochondrial membrane potential was evaluated with the fluorescent probe Rhodamine-123 (Sigma-Aldrich). MDA-MB-231 cells in the density of $2{\cdot}10^4$ were seeded for 24 h in complete medium on 96-well plates, and then treated with various concentrations (0–20 μM) of conjugate **1** or cisplatin for 24 h. Untreated cells contained maximal concentration of DMSO used in the treatment (0.4%). After the treatment, the cells were incubated with Rhodamine-123 dye (1 μM) for 15 min at room temperature and scanned using a FLUOstar Omega spectrofluorometer with excitation and emission wavelengths 488 nm and 530 nm, respectively. Experiments were repeated in duplicate using triplicate points per concentration level.

2.14. Apoptosis induction

The apoptotic or necrotic rate of MDA-MB-231 cells upon exposure of conjugate **1** was evaluated using the Fluorescein Isothiocyanate (FITC)-Annexin V/Propidium Iodide (PI) dual staining method. Briefly, MDA-MB-231 cells were seeded in 12 well plates at a density of $2{\cdot}10^5$ cells/well and incubated overnight. Conjugate **1** or cisplatin were added at indicated concentrations for 24 h. The cells were then harvested, washed with PBS, centrifuged and the pellets were resuspended in 185 μL binding buffer. Then, 15 μL of FITC-Annexin-V/PI solution 1:2 were added and the resuspended cell solution was left at room temperature in the dark for 15 min. Cells were analyzed by flow cytometry (Becton Dickinson FACSCalibur) and a total of 10,000 events were acquired in each sample, registering at 620 and 525 nm for PI and Annexin V, respectively, λ_{exc} = 488 nm. Data were analyzed using Flowing Software version 2.5.1. Experiments were repeated in duplicate with $n = 2$ yielding similar results.

2.15. DNA damage induction

DNA damage in response to **1** was evaluated by flow cytometry as described previously in literature [28]. Briefly, MDA-MB-231 cells were seeded in 6-well plates at $2{\cdot}10^5$ cells/well and treated for 24 h with **1** (20 μM), Erlotinib (20 μM) or cisplatin (20 μM) as positive control for DNA damage induction. Cells were then collected by trypsinization, washed with PBS and fixed in 200 μL 0.2% PFA for 5 min. After fixation, cells were pelleted, resuspended in 3% FBS solution containing anti-pH2AX (ser139) FITC-conjugated monoclonal antibody (CR55T33, eBioscience™) at 0.6 μg/mL and incubated for 2 h at room temperature avoiding direct light. The stained cells were analyzed using Becton

Dickinson FACSCalibur flow cytometer with 10,000 acquisitions per sample and registering FL1-H channel, λ_{exc} = 488 nm. Two independent experiments were performed with $n = 2$ yielding similar results.

2.16. Wound healing assay

The wound healing ability of **1** was evaluated in MDA-MB-231 triple negative breast cancer cells using reported literature procedure [27]. Briefly, 1×10^6 cells were seeded in 60 mm cell culture dishes in DMEM having 10% FBS and allowed to grow for 24 h at 37 °C, 5% CO_2 atmosphere in an incubator. A scratch was made in the cell monolayer using a pipette tip (200 µL). The cells were washed 3 times to remove the floating cells and either 0.1% DMF or **1** (1.0 µM) was added to the cells. Images were recorded using an EVON AMG microscope with a 4× objective lens at 0, 6, 24 and 48 h. The experiment was done in triplicate and repeated 3 times. Images were processed with ImageJ software where the area of the scratch was plotted against time to obtain the $t_{1/2}$ value using a linear fit equation.

2.17. Electrophoretic mobility shift assay (EMSA)

The pBR322 plasmid DNA of 0.25 µg/µl concentration was used for the experiments. 4 µl of charge maker (Lambda–pUC Mix marker, 4) was added to aliquots parts of 20 µl of the drug–DNA complex. The gold complex was incubated at the molar ratio ri = 0.50 with pBR322 plasmid DNA at 37 °C for 24 h. The mixtures underwent electrophoresis in agarose gel 1% in 1× TBE buffer (45 mM Tris-borate,1 mM EDTA, pH 8.0) for 5 h at 30 V. Gel was subsequently stained in the same buffer containing ethidium bromide (1 µg/ml) for 20 min. The DNA bands were visualized with an AlphaImager EC (Alpha Innotech).

2.18. Reactions of 1 with 9-ethylguanine nucleobase followed by ESI-MS

The reaction was carried out in chromatography tubes with DMF 50% as solvent. 9-Ethylguanine was incubated with the complex in a ratio 5:1 in DMF:H_2O at RT. The concentration of the complex was 50 µM.

2.19. Absorption spectroscopic studies

The interaction of complex **1** with calf-thymus DNA has been studied by UV spectroscopy. A series of complex-DNA solutions were prepared by mixing complex stock solution (1.25 mM in DMF) with increasing amounts of calf-thymus DNA stock solution (650 µM in Tris-HCl 5 mM pH 7.2). The final concentration of complex remained fixed at 50 µM.

2.20. ROS induction assay

MDA-MB-231 cells in the density of 2×10^4 per well were seeded for 24 h in 200 µL per well complete medium without Phenol Red on 96-well black plates. Cells were then washed with PBS and incubated with 10 µM 2′,7′-dichlorodihydrofluorescein diacetate (DCFH-DA) for 30 min at 310 K. After incubation, DCFH-DA solution was removed, and gold compounds diluted in cell culture medium without phenol red were added to the cells at appropriate concentrations for 2 h. N-acetylcysteine (NAC) was used a ROS scavenger at 2 mM whereas hydrogen peroxide (H_2O_2) was used as a positive control for ROS production at 200 µM. Fluorescence of DCF product was measured using FLUOstar Omega spectrofluorometer. Two independent experiments were performed with n = 3 replicates.

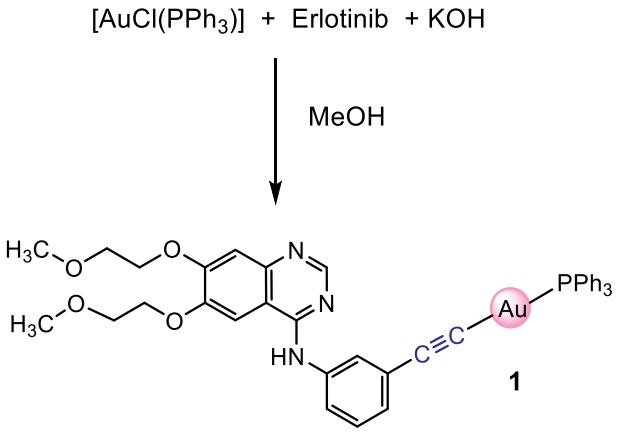

Scheme 1. Synthesis of the gold(I)-Erlotinib conjugate **1**.

3. Results and discussion

3.1. Synthesis and characterization of the Au(I) compound with Erlotinib

The new phosphane gold(I) acetylide complex was prepared by treatment of [AuCl(PPh_3)] with the terminal acetylene Erlotinib in basic conditions (Scheme 1). The structure was studied in solution by NMR, HRMS, UV/Vis and emission spectroscopy, and the high purity needed for biological evaluation was confirmed by elemental analyses. The ^{31}P NMR spectrum showed a unique resonance for coordinated PPh_3 ligand (Fig. S3) and its positive ion ESI-MS spectrum displayed an ion cluster at m/z of 852.227 ($[M + H]^+$, 100%), in agreement with the calculated isotopic pattern. The UV/Vis spectrum displays a set of structured π–π* transition between 250 and 290 nm and another one centered at 334 nm attributed to the quinazolin moiety of Erlotinib (Fig. S5). Both Erlotinib and conjugate **1** have a maxima excitation at 340 nm in aerated DMSO solution and exhibit a high-energy emission centered at 480 and 491 nm, respectively (Fig. S6 and S7). Coordination of Erlotinib to gold(I) comes with a slight red-shift of the emission maxima but the similarity between both the absorption and emission spectra demonstrate that the spectroscopic properties of conjugate **1** are essentially dominated by the ligand.

The stability of conjugate **1** was assessed by UV/Vis spectroscopy over 24 h (Fig. S8) in DMF and 1:1 mixtures of DMF/H_2O and DMF/RPMI culture medium. No changes were observed over the course of the experiment and non-additional bands were detected in the region of 500 nm, characteristic of colloidal gold(0) [14]. In addition, the ^{1}H NMR of **1** in DMSO-d_6 remained stable for > 48 h (Fig. S9). The results demonstrated that the gold compound is stable for further biological testing.

Single crystals of crystallographic formula $C_{40}H_{37}AuN_3O_4P{\cdot}0.413CH_2Cl_2$ (a supramolecular dimer of **1**) suitable for X-ray diffraction analysis were obtained from dicloromethane/toluene/hexane. Crystallographic data are given in Tables S1–S3. The structure (Fig. 1 and Fig. S10) consists of two crystallographically independent monomeric molecules in the unit cell and a partially occupied methylene chloride solvent molecule. Metallo-helicate formation is apparently due to N–H···π(C≡C) or N–H···C^-–Au interactions (H(N4)···C1, 2.62 Å; H(N1)···C41, 2.72 Å; the H···C≡C-centroid contact is 0.1–0.2 Å longer). Each gold atom is coordinated to a phosphane and an alkynyl ligands in an approximately linear manner [C1–Au1–P1, 174.96(8)°; C41–Au2–P2, 174.68(8)°]. The C≡C [C1–C2, 1.206(4) Å; C41–C42 1.206(4) Å], C−Au [Au1–C1, 1.998(3) Å; Au2–C41, 1.991(3) Å] and Au−P [Au1–P1, 2.2717(7) Å; Au2–P2, 2.2721 (7) Å] bond distances are similar to those found in other alkynyl(phosphane)gold(I) complexes [29]. No aurophilic bonds between the two gold(I) centers are observed (Au1···Au2 distances > 6.85 Å).

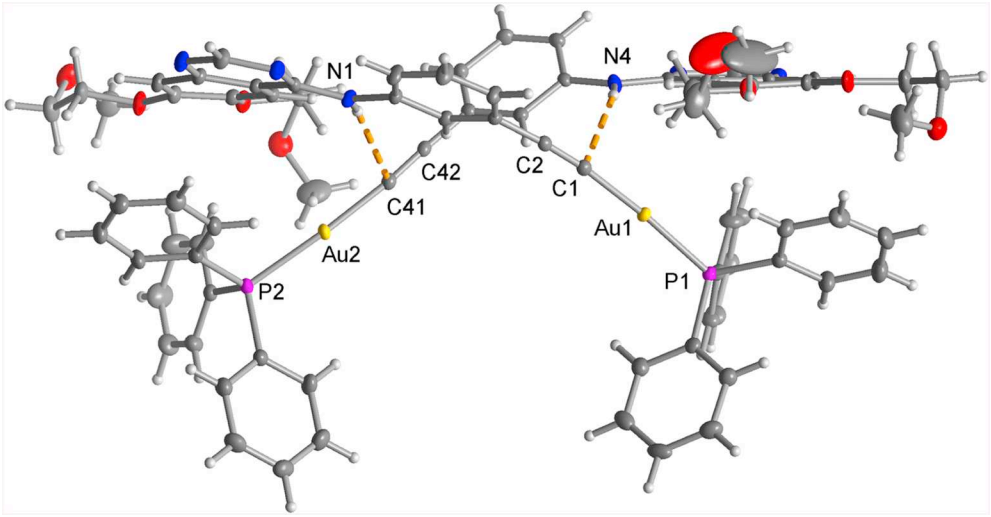

Fig. 1. A view of the supramolecular dimer of **1**, $C_{40}H_{37}AuN_3O_4P$, with partial atom numbering (see Fig. S10 for graphics of the two molecules with full atom numbering).

Table 1
Mean ± SD of IC_{50} values [μM] of **1**, Erlotinib and Auranofin in cancer and normal cell lines.

	HT-29	MCF-7	MDA-MB-231	RC-124	BGM
Erlotinib	> 100	> 100	68.11 ± 11.15	3.14 ± 0.05	> 100
1	3.90 ± 0.12	2.62 ± 0.17	1.64 ± 0.13	0.96 ± 0.28	17.4 ± 1.82
Auranofin	3.79 ± 0.18[a]	2.00 ± 0.05[a]	1.54 ± 0.12[a]	1.44 ± 0.03[a]	–

[a] Source of auranofin IC_{50} values [26].

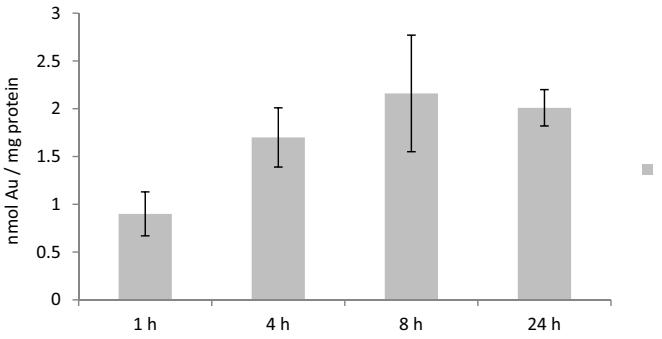

Fig. 2. Cellular uptake of 2.0 μM of **1** into MDA-MB-231 cells, expressed as nmol Au per mg of protein.

3.2. Cytotoxicity

The antiproliferative activity of conjugate **1** and Erlotinib was evaluated (Table 1) in a panel of breast MCF-7 (EGFR-) and MDA-MB-231 (EGFR+) cancer cells, colon adenocarcinoma cell line HT-29 as well as non-tumorigenic cell lines RC-124 and BGM. Auranofin was also evaluated under the same experimental conditions as a positive drug control. Overall, **1** exhibited higher cytotoxic activity than that of Erlotinib against both cancer and normal cells studied, with IC_{50} values ranging between 1 and 4 μM. These values are within the range of the activities of established cytostatics such as cisplatin, 5-fluorouracil and recently studied gold(I) phosphine derivatives [18]. Particularly, the antiproliferative effect of **1** demonstrated to be 68-fold higher than Erlotinib in highly metastatic MDA-MB-231 cell line, which is a model for triple-negative breast cancer and current treatments often fail from benefit. The higher cytotoxicity of **1** within EGFR overexpressing MDA-MB-231 cancer cells might be explained by its specific intracellular accumulation thanks to the Erlotinib-targeting agent. However, conjugate **1** was also able to kill EGFR-negative cells (MCF-7, RC-124 and BGM cells). This result is in contrast with the Erlotinib's and led us think that the reactive gold complex confers to the conjugate with mechanism of action different from that of the organic pharmacophore. A series of cell-experiments finally proved that assumption.

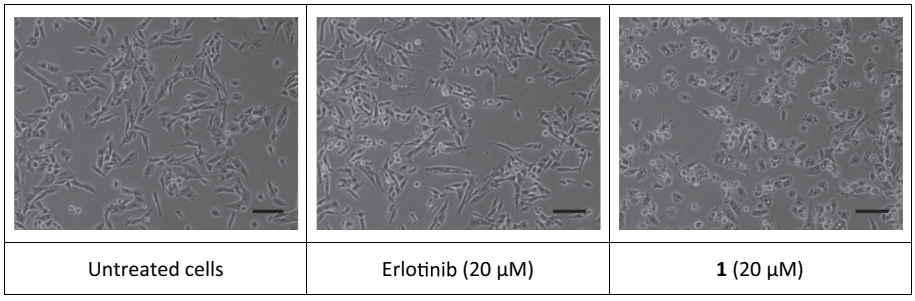

Fig. 3. MDA-MB-231 cells imaged by contrast phase inverted microscopy after treatment with either Erlotinib or **1**. Scale bar: 100 μm.

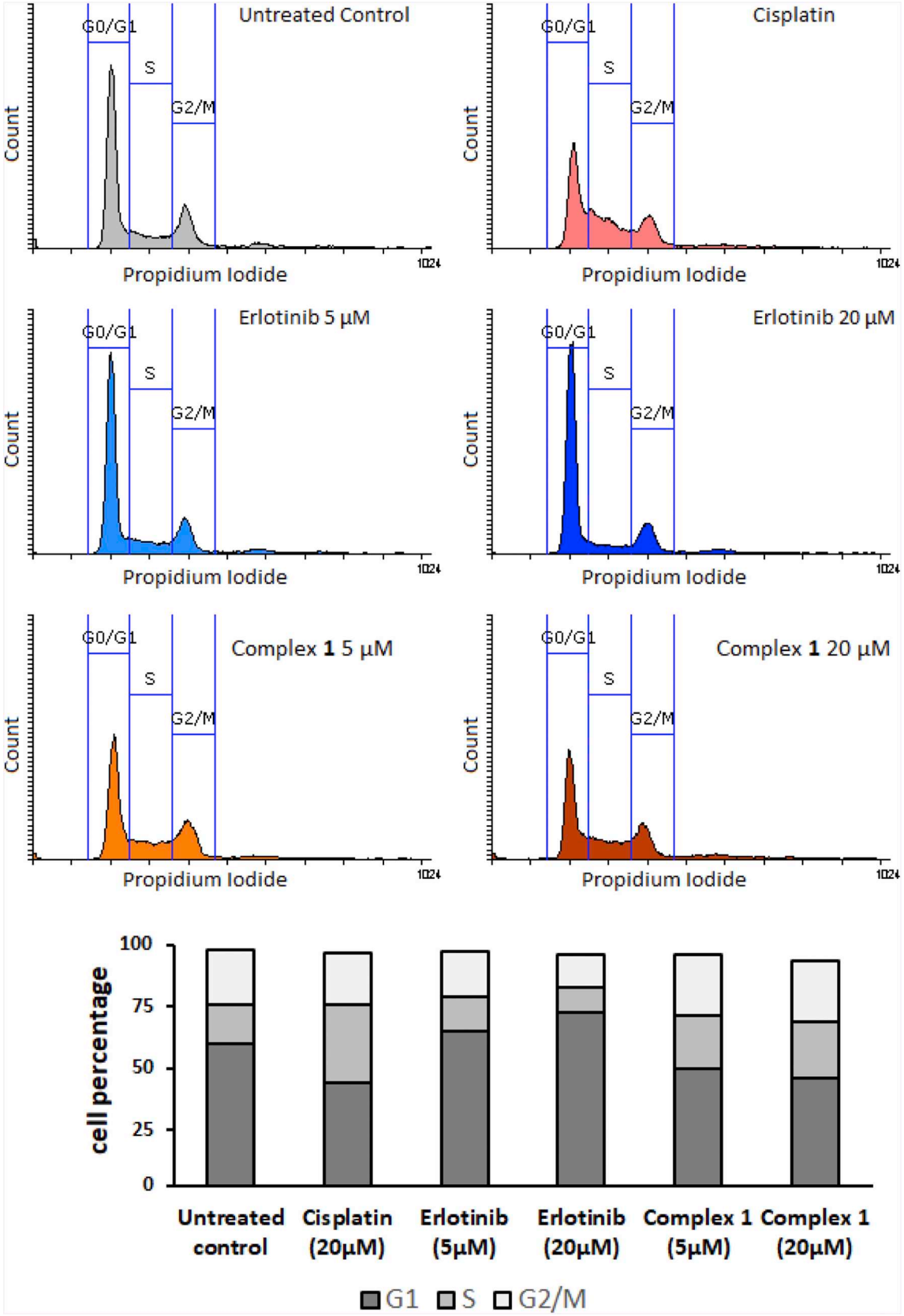

Fig. 4. Cell cycle analysis in MDA-MB-231 cells treated either with Erlotinib or **1** at indicated concentrations. Drug-exposure time was 24 h and the fluorescence intensity of PI was measured in the FL2 channel.

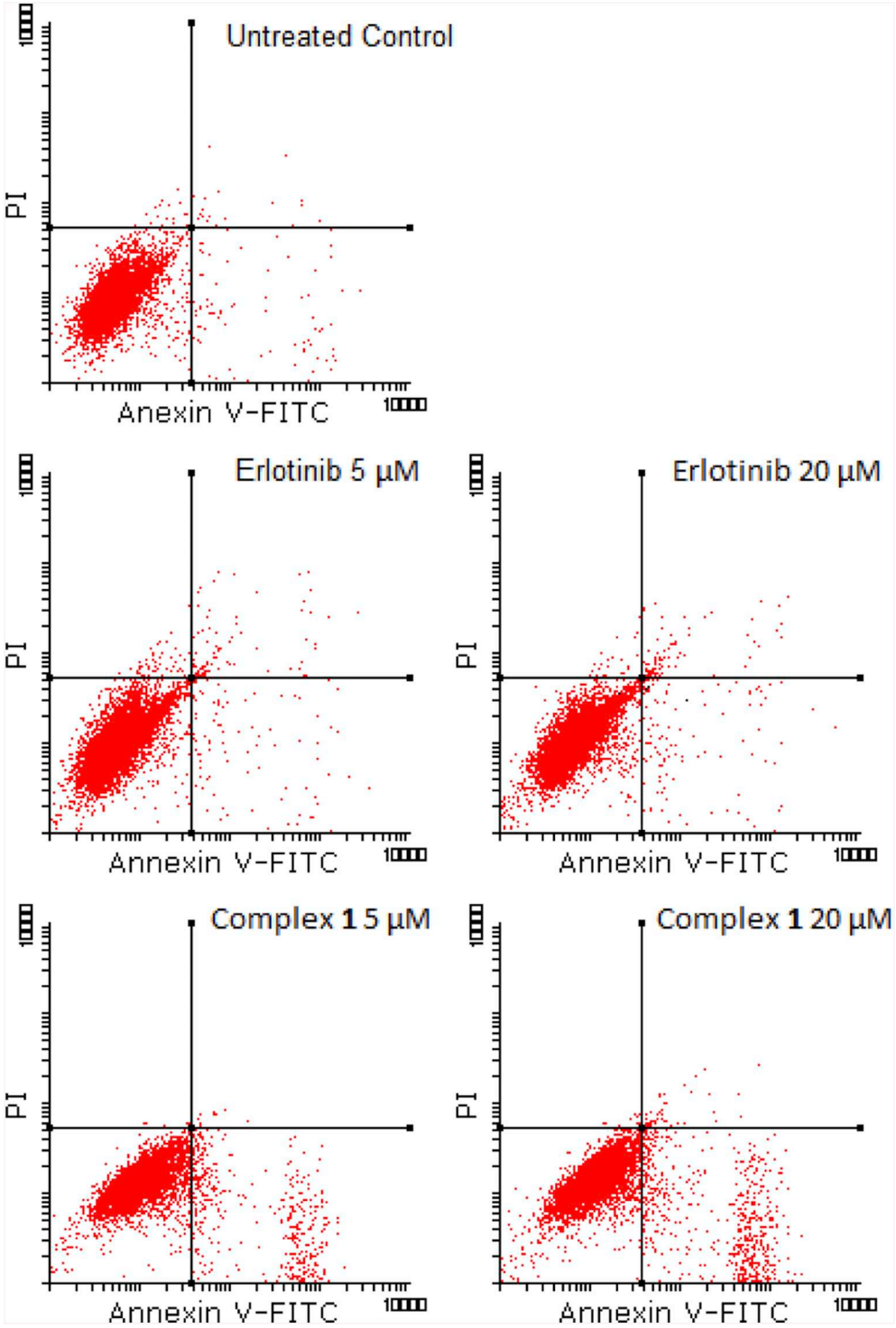

Fig. 5. Dot plots showing Annexin V-FITC/PI dual staining of **1** or Erlotinib treated MDA-MB-231 cells at indicated concentrations for 24 h.

*3.3. Cellular uptake with conjugate **1***

The content of metal inside MDA-MB-231 breast cancer cells was evaluated by AAS upon treatment with 2.0 µM of **1**. The results (Fig. 2) indicate that the cellular uptake of the compound increases over a span of 8 h, reaching a peak of cellular Au accumulation which remains stable over 24 h. The highest values exceeded 2.0 nmol of gold per milligram of cellular protein and were therefore more efficient than that of previously studied gold alkynyl complexes with the triphenylphosphane ligand [18].

3.4. Assessment of cellular morphology changes

The MDA-MB-231 cell line displays endothelial-like morphology with characteristic stellate projections that reflect their invasive phenotype. Treatment with Erlotinib 20 µM resulted in cell death with little to no variation in MDA-MB-231 cell morphology after 24 h compared to the untreated control cells (Fig. 3). However, **1** induced dramatic changes in cellular morphology which included round-shaped cells indicative of metaphase arrest and shrunken cells probably due to apoptosis. In order to verify that **1** inhibits the growth of tumor cells

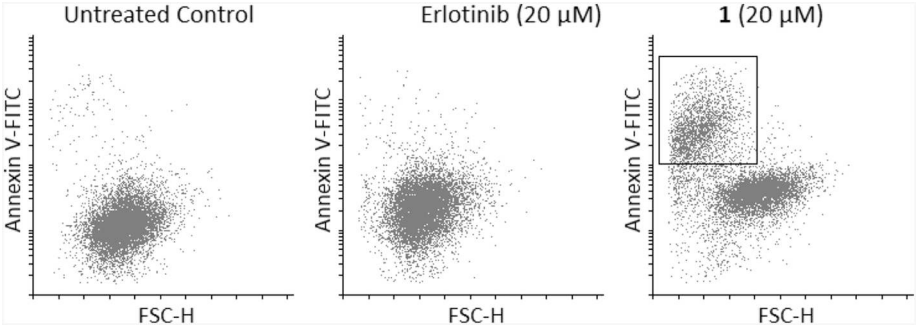

Fig. 6. Relative cell size (FSC-H) versus Annexin V binding capacity of MDA-MB-231 cells treated with **1** or Erlotinib for 48 h. Shrunken cell population with high Annexin V binding capacity is depicted by a rectangular region.

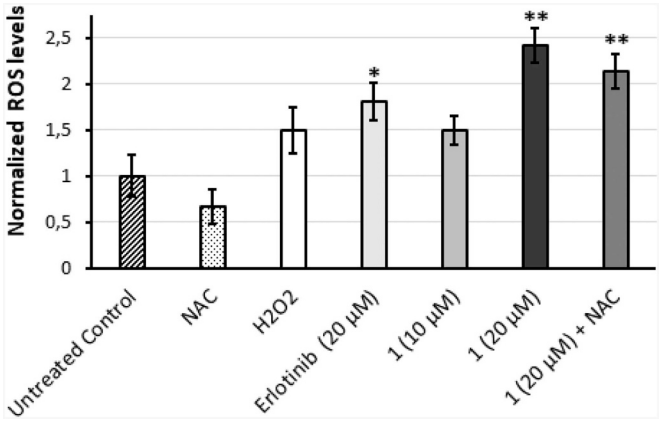

Fig. 7. Fluorescence intensities of DCF measured by flow cytometry in MDA-MB-231 cells treated for 2 h with **1** or Erlotinib at indicated concentrations. *N*-acetyl-cysteine (NAC) was used a ROS scavenger at 2 mM. Statistical data are shown as mean ± SD $^{*}p < .05$, $^{**}p < .01$ (unpaired *t*-test, $n = 3$).

causing the observed morphological changes through cell cycle arrest and apoptosis induction, we conducted flow cytometry experiments (Sections 3.6 and 3.8, respectively).

3.5. Cell death in cancer cells vs. normal cells

Cell death effects were measured in cancer cells and in non-tumoral renal BGM cells by flow cytometry. Exposure of MDA-MB-231 cells to 5 μM of **1** for 24 h did not induce significant changes respect to Erlotinib at equimolar concentration or the untreated control. However, an increase in the fluorescence signal of the FL2 channel for propidium iodide (PI), a fluorescence indicator for cell viability that depends on membrane permeability, was observed for **1** but not for Erlotinib when 20 μM treatment was applied (Fig. S11). This suggests that **1** causes effective cell death at 20 μM compromising membrane integrity of cancer cells. In addition, **1** induced ~25% cell death in cancer cells compared to ~5% observed in non-tumoral BGM cells. This is in agreement with IC_{50} values and suggests that **1** could be less toxic in normal renal cells than in highly metastatic cancer cells.

3.6. Cell cycle analysis

The effect of **1** and Erlotinib on cell cycle was explored in MDA-MB-231 breast cancer cells after 24 h of treatment with either 5 or 20 μM of the compounds. Flow cytometry analysis showed that Erlotinib, as an inhibitor of EGFR, blocked G1/S transition and increases G1 cell population whereas **1** induced a significant arrest in S and G_2/M phases primarily (Fig. 4). Intriguingly, the **1**-FACS profile distribution resembled that of cisplatin, a well-known DNA damaging agent which arrests the cell cycle in these phases. The results suggest that **1** does not act via EGFR inhibition, which would expectedly cause G1 arrest, but rather through a mode of action that might implicate S and G_2/M arrest. As one of the main factors that contribute to S and G_2/M arrest is the DNA damage response pathway [30], we assessed the DNA damage caused by **1** and whether the canonical ROS were involved (Sections 3.10 and 3.9, respectively).

3.7. Mitochondrial membrane potential perturbation

Reduction in mitochondrial membrane potential (MMP) is related to activation of the apoptotic cascade. To study the effect of **1** on MMP, Rhodamine123 staining was carried out in MDA-MB-231 cells after treatment with the conjugate at 5 and 20 μM for 24 h. Fluorescence intensity measurements showed a decrease in MMP upon treatment with either **1** or Erlotinib, indicating that cell death induction could be related to loss of MMP and subsequent intrinsic apoptosis activation (Fig. S12).

3.8. Apoptosis induction

The Annexin V-FITC/PI dual staining was performed in order to determine whether apoptosis or necrosis was the main mechanism of cell death induced by **1**. MDA-MB-231 cells were treated with either **1** or Erlotinib for 24 and 48 h (Fig. 5 and S13, respectively).

Flow cytometry results revealed a positive staining for Annexin V-FITC at 24 h in **1**-treated cells whereas Erlotinib was unable to induce apoptosis at equimolar concentrations. Interestingly, treatment with **1** for 48 h revealed a cell population with high Annexin V binding capacity, suggesting that both cell shrinkage and reduction in cell volume are taking place as a result of apoptotic activation rather than necrosis (Fig. 6).

3.9. ROS generation

We also evaluated whether exposure of cells to **1** generated intracellular reactive oxygen species (ROS) by flow cytometry using 2′,7′-Dichlorodihydrofluorescein diacetate (DCFH-DA) probe, which is intracellularly converted to the fluorescent product 2′,7′-dichlorofluorescein (DCF) by ROS [31]. No changes in ROS levels were observed at 5 μM of either Erlotinib or **1** (data not shown). However, a dose-dependent increase in ROS levels was observed after 2 h incubation with 10 and 20 μM of **1** (Fig. 7 and Fig. S14). Induced ROS generation was slightly attenuated in presence of the ROS scavenger *N*-acetyl-cysteine (NAC). These results indicate that **1** is capable of rapidly rising ROS levels. Mitochondria are one of the major sources of ROS within cells. An increase in the ROS levels prompts the dissipation of the mitochondrial membrane potential and leads to the organelle dysfunction

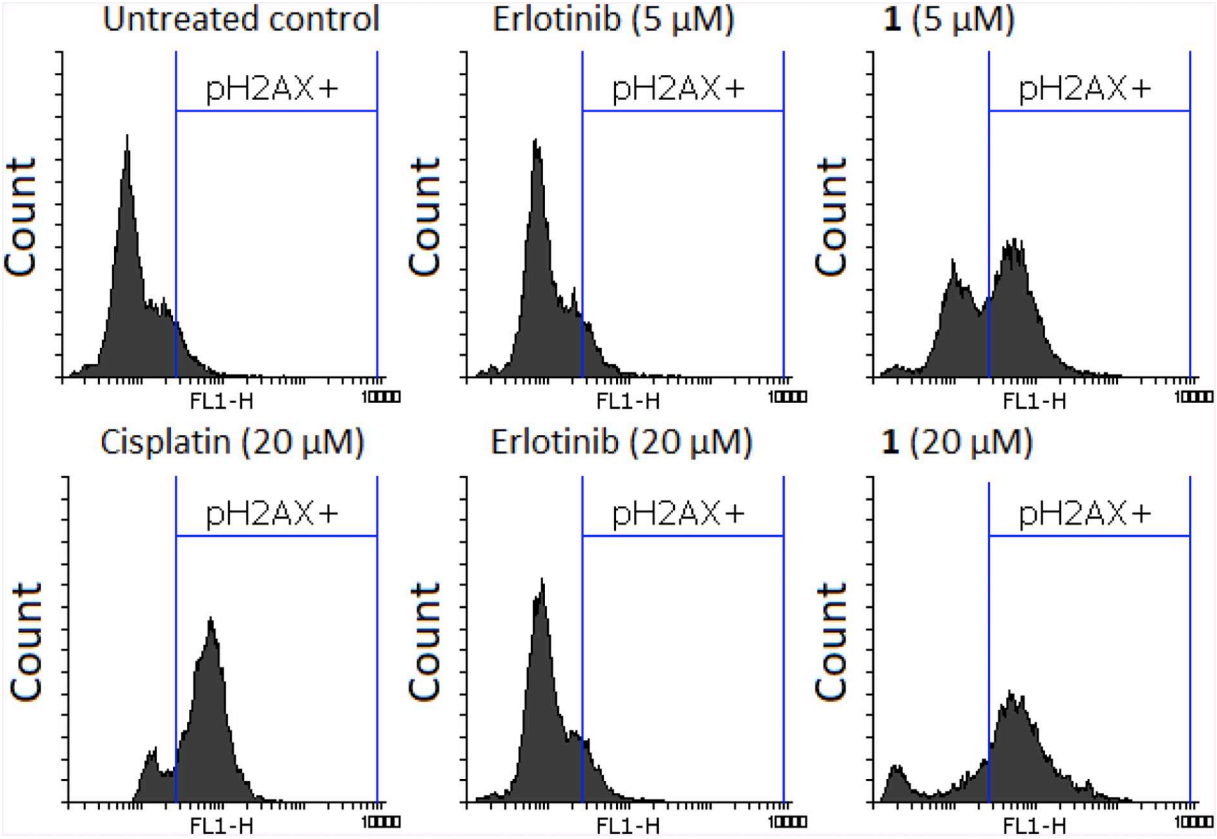

Fig. 8. Effect of **1** and Erlotinib on DNA damage measured by changes in γH2AX phosphorylation in the FL1-H channel after 24 h treatment in MDA-MB-231 cells. Cisplatin was used as a positive control for DNA damage induction.

[32]. Excessive ROS levels have also been linked to DNA damage through the activation of the DNA damage response [33].

3.10. DNA damage in cancer cells

Since ROS is a known contributor of DNA damage, we explored the possibility that **1** could be acting as a DNA interacting compound. For that purpose, isolated nuclear DNA was subjected to ICP-MS for quantitative measurement of gold or platinum content after 24 h treatment of MDA-MB-231 cells with 10 μM of **1** or cisplatin. The Au content bound to DNA in **1**-treated cells (93.3 ± 6.8 pg/μg of DNA) was approximately 3-fold greater than Pt found in cisplatin-treated cells (30.5 ± 4.1 pg/μg DNA). This suggested that **1** might act as a DNA-targeting agent, which is consistent with the cell cycle blockade in S and G_2/M phase.

Next, we investigated the induction of DNA damage breaks upon treatment. We used anti-pH2AX (ser 139) FITC-conjugated antibody to detect DNA double-strand breaks inside cells. The G2/M arrest can be promoted by DNA damage response pathway, which involves double-strand breaks through ROS production. Interestingly, our results showed treatment with **1** but not with Erlotinib induced DNA damage in cancer cells (Fig. 8). At this point, we could hypothesize that extensive DNA damaged cells could undergo cell death via apoptosis.

Moreover, fluorescent indicator displacement assay (Fig. S15) with ethidium bromide (EtBr), competitive binding experiments with Calf Thymus DNA (Fig. S16), reaction with 9-ethylguanine nucleobase followed by ESI-MS (Fig. S17) and EMSA with pBR322 plasmid DNA (Fig. S18) were performed to study DNA-complex interactions. Under the experimental conditions, the interaction with DNA was not observed, which suggests that conjugate **1** might be interacting with this macromolecule in cells by other mechanism rather than covalent binding. Nevertheless, further experimental research will be needed to fully characterize the mode of binding of the conjugate to DNA.

3.11. Wound healing assay

Cell migration is an important step in tumor metastasis [22]; therefore, we performed wound-healing assays to determine the effects of **1** on highly metastatic triple negative MDA-MB-231 breast cancer cell migration. Conjugate **1** was found to delay the rate of wound healing in MDA-MB-231 cell line (Fig. S19). The $t_{1/2}$ (time taken for closure of half the wound) was calculated to be 46.7 ± 4.7 h while the untreated cells had a $t_{1/2}$ value of 32.5 ± 1.8 h.

4. Conclusions

A novel Erlotinib triphenylphosphane gold(I) conjugate **1**, designed to have a high affinity for well-known biological target EGFR, has been synthesized and characterized by X-ray diffraction. The cytotoxicity of the gold conjugate is 68-fold higher than Erlotinib in highly metastatic and triple negative MDA-MB-231 cell line. Contrast phase inverted microscopy studies showed dramatic changes in cellular morphology induced by **1**. Flow cytometry analysis and cell-based fluorescent assays showed that **1** is able to rise the intracellular ROS levels. Subsequent to the production of ROS in cancer cells, the conjugate induced mitochondrial dysfunction and DNA damage, leading to the observed S and G_2/M arrest and eventually to apoptosis activation. Whereas Erlotinib is known to inhibit EGFR tyrosine kinase activity and induce G_1-phase arrest, this paper demonstrated that chemical introduction of a phosphane gold(I) scaffold to the Erlotinib pharmacophore dramatically changed the bioactivity of the resultant conjugate which exerted a different mechanism of action that has been elucidated. In order to

increase selectivity for cancer vs. non-cancer cells an extensive SAR study on new Erlotinib gold(I) conjugates, modifying the nature of the co-ligand (i.e., phosphane and *N*-heterocyclic carbene type ligands with different lipophilicities and/or electronic properties), is currently in progress and will be published in a separate communication.

Acknowledgments

This work was supported by the Spanish Ministerio de Ciencia, Innovación y Universidades and FEDER funds (Projects CTQ2015-64319-R and RTI2018-096891-B-I00) and Fundación Séneca-CARM (Project 20857/PI/18). A.Z. thanks the Fundación Séneca-CARM for a grant (20236/PD/17). Financial support by DFG (Deutsche Forschungsgemeinschaft) is gratefully acknowledged (project number 240296617).

Declaration of competing interest

There is no interest conflict in this paper.

Appendix A. Supplementary data

CCDC 1937968 contains the supplementary crystallographic data for conjugate **1**. These data can be obtained free of charge from The Director, CCDC, 12 Union Road, Cambridge CB21EZ, UK(fax: (+44) 1223–336,033; e-mail: deposit@ccdc.cam.ac.uk or http://www.ccdc.cam.ac.uk). Supplementary data to this article can be found online at https://doi.org/10.1016/j.jinorgbio.2019.110910.

References

[1] F. Bray, J. Ferlay, I. Soerjomataram, R.L. Siegel, L.A. Torre, A. Jemal, Global cancer statistics 2018: GLOBOCAN estimates of incidence and mortality worldwide for 36 cancers in 185 countries, CA Cancer J. Clin. 68 (2018) 394–424, https://doi.org/10.3322/caac.21492.

[2] K. Hongthong, A. Ratanaphan, BRCA1-associated triple-negative breast Cancer and potential treatment for ruthenium-based compounds, Curr. Cancer Drug Targets 16 (2016) 606–617.

[3] Y. Yarden, The EGFR family and its ligands in human cancer: signalling mechanisms and therapeutic opportunities, Eur. J. Cancer 37 (2001) 3–8, https://doi.org/10.1016/S0959-8049(01)00230-1.

[4] J. Dowell, J.D. Minna, P. Kirkpatrick, Erlotinib hydrochloride, Nat. Rev. Drug Discov. 4 (2005) 13–14, https://doi.org/10.1038/nrd1612.

[5] S. Dasari, P.B. Tchounwou, Cisplatin in cancer therapy: molecular mechanisms of action, Eur. J. Pharmacol. 740 (2014) 364–378, https://doi.org/10.1016/j.ejphar.2014.07.025.

[6] B. Bao, C. Mitrea, P. Wijesinghe, L. Marchetti, E. Girsch, R.L. Farr, J.L. Boerner, R. Mohammad, G. Dyson, S.R. Terlecky, A. Bollig-Fischer, Treating triple negative breast cancer cells with erlotinib plus a select antioxidant overcomes drug resistance by targeting cancer cell heterogeneity, Sci. Rep. 7 (2017) 44125, , https://doi.org/10.1038/srep44125.

[7] S. Jurgens, F.E. Kuhn, A. Casini, Cyclometalated complexes of platinum and gold with biological properties: state-of-the-art and future perspectives, Curr. Med. Chem. 25 (2018) 437–461, https://doi.org/10.2174/0929867324666170529125229.

[8] M. Mora, M.C. Gimeno, R. Visbal, Recent advances in gold–NHC complexes with biological properties, Chem. Soc. Rev. 48 (2019) 447–462, https://doi.org/10.1039/C8CS00570B.

[9] A. Casini, R.W.-Y. Sun, I. Ott, Medicinal chemistry of gold anticancer metallodrugs, Met Ions Life Sci. 18 (2018) 199–217, https://doi.org/10.1515/9783110470734-013.

[10] E. García-Moreno, A. Tomás, E. Atrián-Blasco, S. Gascón, E. Romanos, M.J. Rodriguez-Yoldi, E. Cerrada, M. Laguna, In vitro and in vivo evaluation of organometallic gold(I) derivatives as anticancer agents, Dalton Trans. 45 (2016) 2462–2475, https://doi.org/10.1039/C5DT01802A.

[11] A.D. Nisi, C. Bergamini, M. Leonzio, G. Sartor, R. Fato, M. Naldi, M. Monari, N. Calonghi, M. Bandini, Synthesis, cytotoxicity and anti-cancer activity of new alkynyl-gold(I) complexes, Dalton Trans. 45 (2016) 1546–1553, https://doi.org/10.1039/C5DT02905H.

[12] C.-H. Chui, R.S.-M. Wong, R. Gambari, G.Y.-M. Cheng, M.C.-W. Yuen, K.-W. Chan, S.-W. Tong, F.-Y. Lau, P.B.-S. Lai, K.-H. Lam, C.-L. Ho, C.-W. Kan, K.S.-Y. Leung, W.-Y. Wong, Antitumor activity of diethynylfluorene derivatives of gold(I), Bioorg. Med. Chem. 17 (2009) 7872–7877, https://doi.org/10.1016/j.bmc.2009.10.034.

[13] V. Scalcon, A. Bindoli, M.P. Rigobello, Significance of the mitochondrial thioredoxin reductase in cancer cells: an update on role, targets and inhibitors, Free Radic. Biol. Med. 127 (2018) 62–79, https://doi.org/10.1016/j.freeradbiomed.2018.03.043.

[14] I. Mármol, M. Virumbrales-Muñoz, J. Quero, C. Sánchez-de-Diego, L. Fernández, I. Ochoa, E. Cerrada, M.J.R. Yoldi, Alkynyl gold(I) complex triggers necroptosis via ROS generation in colorectal carcinoma cells, J. Inorg. Biochem. 176 (2017) 123–133, https://doi.org/10.1016/j.jinorgbio.2017.08.020.

[15] C. Sánchez-de-Diego, I. Mármol, R. Pérez, S. Gascón, M.J. Rodriguez-Yoldi, E. Cerrada, The anticancer effect related to disturbances in redox balance on Caco-2 cells caused by an alkynyl gold(I) complex, J. Inorg. Biochem. 166 (2017) 108–121, https://doi.org/10.1016/j.jinorgbio.2016.11.009.

[16] V. Andermark, K. Göke, M. Kokoschka, M.A. Abu el Maaty, C.T. Lum, T. Zou, R.W.-Y. Sun, E. Aguiló, L. Oehninger, L. Rodríguez, H. Bunjes, S. Wölfl, C.-M. Che, I. Ott, Alkynyl gold(I) phosphane complexes: evaluation of structure–activity-relationships for the phosphane ligands, effects on key signaling proteins and preliminary in-vivo studies with a nanoformulated complex, J. Inorg. Biochem. 160 (2016) 140–148, https://doi.org/10.1016/j.jinorgbio.2015.12.020.

[17] N. Mirzadeh, S.H. Privér, A. Abraham, R. Shukla, V. Bansal, S.K. Bhargava, Linking flavonoids to gold – a new family of gold compounds for potential therapeutic applications, Eur. J. Inorg. Chem. 2015 (2015) 4275–4279, https://doi.org/10.1002/ejic.201500514.

[18] A. Meyer, C.P. Bagowski, M. Kokoschka, M. Stefanopoulou, H. Alborzinia, S. Can, D.H. Vlecken, W.S. Sheldrick, S. Wölfl, I. Ott, On the biological properties of alkynyl phosphine gold(I) complexes, Angew. Chem. Int. Ed. 51 (2012) 8895–8899, https://doi.org/10.1002/anie.201202939.

[19] V. Ganga Reddy, T. Srinivasa Reddy, S.H. Privér, Y. Bai, S. Mishra, D. Wlodkowic, N. Mirzadeh, S. Bhargava, Synthesis of gold(I) complexes containing cinnamide: in vitro evaluation of anticancer activity in 2D and 3D spheroidal models of melanoma and in vivo angiogenesis, Inorg. Chem. 58 (2019) 5988–5999, https://doi.org/10.1021/acs.inorgchem.9b00281.

[20] F.-L. Zhang, Q. Huang, K. Zheng, J. Li, J.-Y. Liu, J.-P. Xue, A novel strategy for targeting photodynamic therapy. Molecular combo of photodynamic agent zinc(II) phthalocyanine and small molecule target-based anticancer drug erlotinib, Chem. Commun. 49 (2013) 9570–9572, https://doi.org/10.1039/C3CC45487H.

[21] R. Uson, A. Laguna, M. Laguna, D.A. Briggs, H.H. Murray, J.P. Fackler, (Tetrahydrothiophene)Gold(I) or Gold(III) Complexes, in: Inorganic Syntheses, John Wiley & Sons, Ltd., 2007, pp. 85–91, https://doi.org/10.1002/9780470132579.ch17.

[22] S.A. Pérez, C. de Haro, C. Vicente, A. Donaire, A. Zamora, J. Zajac, H. Kostrhunova, V. Brabec, D. Bautista, J. Ruiz, New acridine thiourea gold(I) anticancer agents: targeting the nucleus and inhibiting Vasculogenic mimicry, ACS Chem. Biol. 12 (2017) 1524–1537, https://doi.org/10.1021/acschembio.7b00090.

[23] G.M. Sheldrick, A short history of SHELX, Acta Cryst. A. 64 (2008) 112–122, https://doi.org/10.1107/S0108767307043930.

[24] G.M. Sheldrick, SADABS, Program for Empirical Absorption Correction of Area Detector Data, Universität Göttingen, Göttingen, 1996.

[25] T.R. Chen, Microscopic demonstration of mycoplasma contamination in cell cultures and cell culture media, Tca Manual 1 (1975) 229–232, https://doi.org/10.1007/BF00917008.

[26] C. Schmidt, B. Karge, R. Misgeld, A. Prokop, M. Brönstrup, I. Ott, Biscarbene gold(I) complexes: structure–activity-relationships regarding antibacterial effects, cytotoxicity, TrxR inhibition and cellular bioavailability, Med. Chem. Commun. 8 (2017) 1681–1689, https://doi.org/10.1039/C7MD00269F.

[27] C.-C. Liang, A.Y. Park, J.-L. Guan, *In vitro* scratch assay: a convenient and inexpensive method for analysis of cell migration *in vitro*, Nat. Protoc. 2 (2007) 329–333, https://doi.org/10.1038/nprot.2007.30.

[28] A. Muslimovic, I.H. Ismail, Y. Gao, O. Hammarsten, An optimized method for measurement of gamma-H2AX in blood mononuclear and cultured cells, Nat. Protoc. 3 (2008) 1187–1193, https://doi.org/10.1038/nprot.2008.93.

[29] E. Vergara, E. Cerrada, A. Casini, O. Zava, M. Laguna, P.J. Dyson, Antiproliferative activity of gold(I) alkyne complexes containing water-soluble phosphane ligands, Organometallics 29 (2010) 2596–2603, https://doi.org/10.1021/om100300a.

[30] D. Branzei, M. Foiani, Regulation of DNA repair throughout the cell cycle, Nat Rev Mol Cell Biol 9 (2008) 297–308, https://doi.org/10.1038/nrm2351.

[31] J.J. González, E. Ortega, M. Rothemund, M. Gold, C. Vicente, C. de Haro, D. Bautista, R. Schobert, J. Ruiz, Luminescent gold(I) complexes of 1-pyridyl-3-anthracenylchalcone inducing apoptosis in Colon carcinoma cells and Antivascular effects, Inorg. Chem. 58 (2019) 12954–12963, https://doi.org/10.1021/acs.inorgchem.9b01901.

[32] D. Trachootham, J. Alexandre, P. Huang, Targeting cancer cells by ROS-mediated mechanisms: a radical therapeutic approach? Nat. Rev. Drug Discov. 8 (2009) 579–591, https://doi.org/10.1038/nrd2803.

[33] U.S. Srinivas, B.W.Q. Tan, B.A. Vellayappan, A.D. Jeyasekharan, ROS and the DNA damage response in cancer, Redox Biol. (2018) 101084, , https://doi.org/10.1016/j.redox.2018.101084.